

Are There Different Populations of Flux Ropes in the Solar Wind?

M. Janvier · P. Démoulin · S. Dasso

Received: 10 November 2013 / Accepted: 1 February 2014 / Published online: 4 March 2014
© Springer Science+Business Media Dordrecht 2014

Abstract Flux ropes are twisted magnetic structures that can be detected by *in-situ* measurements in the solar wind. However, different properties of detected flux ropes suggest different types of flux-rope populations. As such, are there different populations of flux ropes? The answer is positive and is the result of the analysis of four lists of flux ropes, including magnetic clouds (MCs), observed at 1 AU. The *in-situ* data for the four lists were fitted with the same cylindrical force-free field model, which provides an estimate of the local flux-rope parameters such as its radius and orientation. Since the flux-rope distributions have a broad dynamic range, we went beyond a simple histogram analysis by developing a partition technique that uniformly distributes the statistical fluctuations across the radius range. By doing so, we found that small flux ropes with radius $R < 0.1$ AU have a steep power-law distribution in contrast to the larger flux ropes (identified as MCs), which have a Gaussian-like distribution. Next, from four CME catalogs, we estimated the expected flux-rope frequency per year at 1 AU. We found that the predicted numbers are similar to the frequencies of MCs observed *in-situ*. However, we also found that small flux ropes are at least ten times too abundant to correspond to CMEs, even to narrow ones. Investigating the different possible scenarios for the origin of these small flux ropes, we conclude that these twisted structures can be formed by blowout jets in the low corona or in coronal streamers.

Keywords Coronal mass ejections · Coronal mass ejections, interplanetary · Magnetic fields, interplanetary · Solar wind

M. Janvier (✉)

Department of Mathematics, University of Dundee, Dundee, DD1 4HN, Scotland, UK
e-mail: mjanvier@maths.dundee.ac.uk

P. Démoulin

Observatoire de Paris, LESIA, UMR 8109 (CNRS), 92195 Meudon Principal Cedex, France

S. Dasso

Instituto de Astronomía y Física del Espacio, UBA-CONICET, CC. 67, Suc. 28, 1428 Buenos Aires, Argentina

S. Dasso

Departamento de Física, Facultad de Ciencias Exactas y Naturales, UBA, Buenos Aires, Argentina

1. Introduction

The data from *in-situ* measurements made by spacecraft in the heliosphere can show a coherent rotation of the magnetic field on time scales of hours to days. These coherent magnetic structures are typically interpreted as twisted magnetic configurations, commonly called flux ropes (hereafter FRs).

The earliest discovered and most commonly identified FRs were the large ones, with sizes of about 0.1 AU at Earth's orbit (Lepping, Burlaga, and Jones, 1990 and references therein). These FRs are called magnetic clouds (MCs), and they are characterized by a smooth rotation of an enhanced magnetic field and a proton temperature lower than that of the averaged solar wind, while traveling with the same speed (see, *e.g.*, Elliott *et al.*, 2005; Démoulin, 2009). Their physical properties have been analyzed in depth (see, *e.g.*, Dasso *et al.*, 2005; Lynch *et al.*, 2005; Lepping and Wu, 2010). They are seen in a fraction ($\approx 1/3$) of the interplanetary coronal mass ejections (ICMEs) that are defined from a broader set of criteria (including proton temperature, ionisation levels, composition; see Richardson and Cane, 2010, and references therein). With their coronagraphs, heliospheric imagers and *in-situ* measurements, the twin spacecraft of the *Solar Terrestrial Relations Observatory* (STEREO) have unambiguously associated ICMEs with CMEs launched from the Sun (Rouillard, 2011, and references therein).

Similarly, small events are also detected with heliospheric imagers (Rouillard *et al.*, 2010; Sheeley and Rouillard, 2010) as well as in the corona, including eruptions from ephemeral regions and narrow CMEs (Mandrini *et al.*, 2005; Robbrecht, Berghmans, and Van der Linden, 2009; Schrijver, 2010), blowout X-ray jets (Moore *et al.*, 2010, 2013), and streamer blobs (Wang, Zhang, and Shen, 2009; Sheeley *et al.*, 2009). In parallel, much smaller FRs than typical MCs have been detected with *in-situ* measurements (Moldwin *et al.*, 2000). In contrast to MCs, these structures present no significant variations of the proton temperature when they are crossed by spacecraft. In the following, we simply call them "small FRs," while we use "FRs" to refer to all flux ropes detected *in-situ*. The small FRs are fitted with the same flux-rope model as MCs by simply rescaling them in size (Feng, Wu, and Chao, 2007; Cartwright and Moldwin, 2008). Statistical studies of small FRs at various solar distances indicate that small FRs expand as a power law of the solar distance, but with an exponent that is about half the exponent found for MCs (Cartwright and Moldwin, 2010a; Gulisano *et al.*, 2010). However, in contrast to MCs, this expansion is not detected with *in-situ* observations of small FRs (Moldwin *et al.*, 2000; Feng, Wu, and Chao, 2007; Cartwright and Moldwin, 2008; Kilpua *et al.*, 2012).

The question that arises from these different properties is whether MCs and small FRs have the same origin. Moldwin *et al.* (2000) claimed that there are no intermediate sizes between MCs and small FRs. Furthermore, Cartwright and Moldwin (2008, 2010a) argued that the FR distribution is double-peaked with different characteristics for MCs and small FRs from the *in-situ* data (such as the proton temperature and the expansion rate). In contrast, Feng, Wu, and Chao (2007) found a continuous distribution in FR diameters, and Wu, Feng, and Chao (2008) found a power law for the total-energy spectrum with a slope comparable, while smaller, with the slope found in the energy spectrum of solar flares. This debate is also present at a deeper level for the definition of small FRs (Feng, Wu, and Chao, 2010; Cartwright and Moldwin, 2010b): indeed, the lists of small FRs of Feng, Wu, and Chao (2007) and Cartwright and Moldwin (2008) have few cases in common, while they have a large temporal overlap and are observed by the same spacecraft (*Wind*).

In the present study, we propose a deeper analysis of the spectrum of FRs present in the SW from different readily available lists. In Section 2, we describe the four data sets used and their modeling. Then, in Section 3, we analyze the distribution of the FR radius, introducing a new technique for the statistical analysis, and in Section 4 we analyze and correct the biases of the observed distributions. This technique is applied in Section 5 to study small FRs. In Section 6, we separate MCs from small FRs, then in Section 7 we provide evidence that only MCs are related to CMEs. Finally, we investigate the possible origin of small FRs in Section 8. We summarize our results and conclude in Section 9.

2. Description of the Four Flux Rope Lists

We used four lists of FRs observed in the solar wind nearby Earth by the Wind or *Advanced Composition Explorer* (ACE) spacecraft. The first list of FRs, which are mostly MCs, is attached to the article of Lynch *et al.* (2005). It contains 132 FRs observed from February 1995 to November 2003. A second list of FRs is provided in Table 1 of Feng, Wu, and Chao (2007). It contains 144 FRs (of both MCs and small FRs) observed from February 1995 to September 2001. A third list of small FRs is given in Table 1 of Feng *et al.* (2008). It contains 125 small FRs observed from February 1995 to November 2005. Finally, a fourth list of MCs (Table 2 at wind.nasa.gov/mfi/mag_cloud_S1.html) is based on the results of Lepping and Wu (2010) and it provides an extension of the list to more recent MCs. This list, as of 12 July 2013, contains the parameters obtained for 121 MCs observed by the Wind spacecraft from February 1995 to December 2009. The four lists have a comparable number of FRs, but every list spans different spatial and temporal intervals (although they partly overlap). In the following, we study them independently.

Since MCs typically have a low plasma β , they are considered to be in a near force-free-field state. Moreover, since clear FR signatures are present in the *in-situ* data, their magnetic configuration is generally modeled using force-free FR models. The simplest, but still widely used model is the cylindrical linear force-free field (Lundquist, 1950):

$$\mathbf{B}_L = B_0 [J_1(\alpha r) \hat{\mathbf{e}}_\phi + J_0(\alpha r) \hat{\mathbf{e}}_z], \quad (1)$$

where J_0 and J_1 are the ordinary Bessel functions of order 0 and 1, and $\hat{\mathbf{e}}_\phi$ and $\hat{\mathbf{e}}_z$ are the unit vectors in cylindrical coordinates. The axial component of \mathbf{B}_L is typically imposed to vanish at the boundary $r = R$ of the FR, so α is determined by the first zero of J_0 , implying $\alpha \approx 2.4/R$.

The Lundquist model is then used to fit each event in the four lists described above. The least-squares-fitting procedure is the same as, or closely similar to, that used by Lepping, Burlaga, and Jones (1990). Variations of the fitting procedure include the precise algorithm to achieve the nonlinear fit and the choice of the FR boundaries. We refer to the articles cited above for further information on the implementation of the fitting procedure for each list of FRs. The fit to the *in-situ* data determines the seven free parameters of the model (the longitude and the latitude of the FR axis, the distance of the spacecraft from the FR axis at closest approach point, the magnetic-field strength on the FR axis, the twist, the sign of the magnetic helicity, and the time at closest approach to the FR axis). The parameters used here are the flux-rope axis orientation (longitude $[\phi]$ and latitude $[\theta]$), the magnetic-field strength on the FR axis $[B_0]$, and the FR radius $[R]$ deduced from the previous parameters.

3. A New Technique for the Analysis of the FR Distributions

Cartwright and Moldwin (2008) found evidence that the distribution of FRs is double-peaked, with the most numerous FRs having durations shorter than four hours, while the second peak of the distribution, about 12–16 hours, corresponds to MCs. In the following, we analyze the FR distributions in more detail by using the four different lists described above. The temporal duration of a flux-rope crossing depends both on its speed and on its orientation (with a longer crossing time because the spacecraft crossing trajectory is nearly aligned with the FR axis). On the other hand, the FR radius is an intrinsic property of the FR. Therefore, we study in the following only the distributions of the FR radius.

A classical statistical analysis of the distribution of a parameter (here the radius $[R]$) involves histograms with a uniform binning width. The key point of such an analysis is to define a proper number of bins $[N_{\text{bin}}]$. Indeed, the bin width needs to be not too narrow so that there are enough counts in each bin, but must not be too broad either to represent the distribution variations as well as possible. However, when this distribution has a broad range of counts in various bins over a wide range of R , the most suitable bin width cannot be found. This is the case for observed FRs because the selection of a bin width adapted to the MCs implies that small FRs are all set in a few bins (see, *e.g.*, Figure 10 of Cartwright and Moldwin, 2008).

To analyze a distribution that extends over a wide range of radius with strong count variations, the bin size needs to be adapted either to the radius scale or to the FR counts. We selected the latter option as it provides a uniform count, so it decreases and spreads the statistical fluctuations uniformly over all the bins. We proceeded by first ordering the FRs by increasing radius. Next, we defined partitions with N_{part} cases in each. The lowest partition contains the N_{part} cases with the lowest radius. In the next one, the cases are shifted to higher radius by one case only, and so on until the case with the largest radius is incorporated in the last partition. We chose to shift from one partition to the neighboring one by only one case, as the method can be applied to any total number of cases N_{FR} without removing any data (*e.g.* a shift with two cases would remove the FR with the largest radius if N_{FR} were odd). In contrast to a classical histogram, where an FR is only present in one bin, the partition method implies that FRs become present in consecutive partitions except for the first and last ranked FRs. This implies a larger sampling of the distribution function, allowing us to better identify its variations (because there can be more partitions than bins of a histogram).

The distribution $\mathcal{D}(R)$ deduced from a histogram is given by the number of cases $[\Delta N = N(R_2) - N(R_1)]$ in each bin of fixed width $[\Delta R = R_2 - R_1]$:

$$N(R_2) - N(R_1) = \int_{R_1}^{R_2} \mathcal{D}(R) dR \approx \mathcal{D}\left(\frac{R_1 + R_2}{2}\right)(R_2 - R_1). \tag{2}$$

With the partition technique presented above, ΔN is fixed to a value N_{part} while ΔR remains variable. ΔR can be estimated by the boundary values of R for each partition. Performing several tests with randomly generated distributions, we verified that a robust estimation of ΔR is to define it with the standard deviation of R $[\sigma_R]$ for each partition. More precisely, the two quantities are linked by $\Delta R = 2\sqrt{3}\sigma_R$ assuming a uniform distribution in each partition. Using randomly generated distributions confirms that the value of σ_R in a partition is weakly affected by the type of distribution analyzed provided that the partition extension is small compared with the variation of the global distribution. This was also tested with a broad range of synthetic power-law distributions (see Section 5) by analytically computing σ_R and comparing it with the numerical results. We conclude that the estimation of ΔR with σ_R is reliable enough to provide an estimate of the distribution in each partition. In the following, we analyze the distribution $[dN/dR]$ estimated with $N_{\text{part}}/(2\sqrt{3}\sigma_R)$

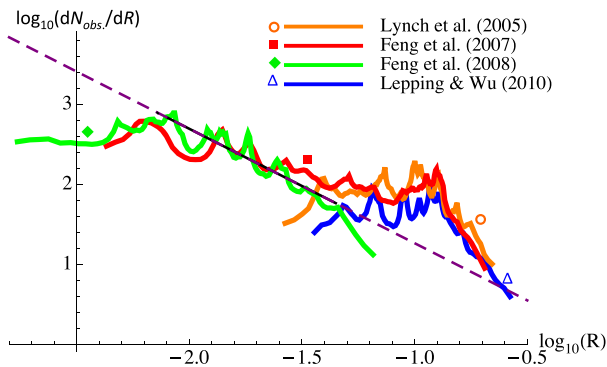


Figure 1 Observed distributions $[dN_{\text{obs}}/dR]$ of flux ropes *versus* the mean FR radius of each partition (see Section 3 for the partition technique), noted here R for simplification in log–log scales. N is the number of cases per year, with a number of cases in each partition being $N_{\text{part}} = 10$, and the FR radius $[R]$ is in AU. The continuous black straight line is the fit of the distribution of small FRs from Feng *et al.* (2008) within the radius range $[0.008, 0.05]$ AU. The fit is extended beyond the fitting region by the dashed purple line.

for each partition *versus* the mean value $\langle R \rangle$, hereafter simply denoted R in the graphs for convenience.

Because the four lists are associated with different temporal ranges (Section 2), we normalized the obtained FR distribution with the number of related years of observation to be able to compare all of the results. Their distributions are shown in Figure 1, for which we have chosen $N_{\text{part}} = 10$ so as to minimize the averaging effect (*i.e.* its possible bias consequences). This low N_{part} value implies statistical fluctuations of ΔR of amplitude $\lesssim 0.2$ in the logarithm. Nevertheless, comparing the distributions of FRs from the different lists, there is a large bump around $R = 0.1$ AU that is much higher than the power-law distribution (indicated in black) of smaller FRs and that cannot be explained simply by statistical fluctuations. The three lists that include MCs nearly agree for high R values (red, orange, and blue curves in Figure 1), although the list of Lepping and Wu (2010) (blue curve) excludes a significant number of MCs below $R \approx 0.1$ AU in contrast to the lists of Lynch *et al.* (2005) and Feng, Wu, and Chao (2007). Finally, a power-law fit of the list of Feng *et al.* (2008) (black line), which is limited to small FRs, shows that the larger FRs, *i.e.* the MCs, are much more numerous than expected with the extension of this power law to a larger radius. We conclude that there are two populations of FRs with different origins (because their distributions are clearly different). We analyze these two distributions in more detail in the next two sections.

4. From Local to Global Probability Distributions

In the intermediate range of radius, dN_{obs}/dR is close to a power law as fitted by the straight line in the log–log plot of Figure 1. However, this power law seems to break down for small radii, especially for the list of Feng *et al.* (2008), which contains the largest number of small FRs. Therefore we investigated whether the global parameters of such small FRs show peculiarities, and whether selection effects play a role in the breaking down of the power law. To do so, we first ordered the FRs with one of the global parameters, then we split the FRs into a few groups, with growing values of the selected parameter. This allowed us to test whether the distributions dN_{obs}/dR are affected by this selected parameter. Because we

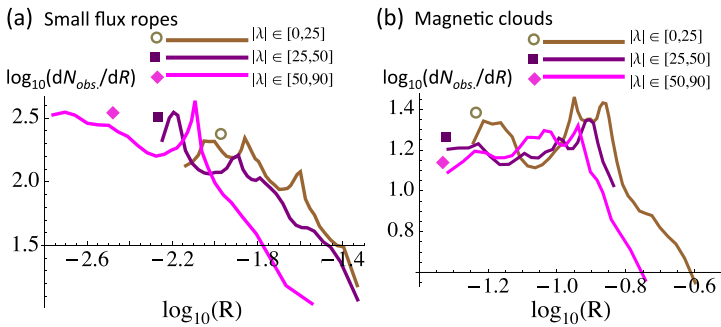


Figure 2 Observed FR distributions $[dN_{obs}/dR]$ versus FR radius in log–log scales split into groups of $|\lambda|$ (angle between the flux-rope axis and the plane orthogonal to the Sun–spacecraft direction, see Equation (3)). The ranges of $|\lambda|$ are selected to have a similar number of FRs for each distribution. (a) Distributions for small FRs (Feng *et al.*, 2008). (b) Distributions for MCs (Lepping and Wu, 2010).

only found a significant effect with the location angle $[\lambda]$, we describe the results obtained below.

The location angle $[\lambda]$ is the angle between the FR-axis direction and the direction orthogonal to the Sun–spacecraft direction (which is the typical direction of the FR propagation; see the schema in Figure 1 of Janvier, Démoulin, and Dasso, 2013). This angle is referred to as a location angle because it directly gives an idea of the position of the spacecraft along the FR axis. Note that λ is related to the longitude $[\phi]$ and latitude $[\theta]$ of the FR axis by the following relation:

$$\sin \lambda = \cos \phi \cos \theta. \tag{3}$$

The location angle $[\lambda]$ becomes 0 for an orthogonal crossing of the FR (spacecraft at the apex of the FR), and $|\lambda|$ increases when the crossing is more aligned along the FR axis. Then, we split the data of Feng *et al.* (2008) into three groups according to their $|\lambda|$ values. The number of groups was limited by the total number of FRs, and we chose the boundaries of the three groups so as to have approximately the same number of FRs and for the corresponding dN_{obs}/dR to be comparable in magnitude and in statistical fluctuations. The amplitude of the statistical fluctuations seen throughout the three distributions shows that the central bump in the distribution of $50^\circ < |\lambda| \leq 90^\circ$ (in purple in Figure 2a) is most likely a statistical fluctuation. Figure 2a shows that the slope for large $\log R$ is similar for the three different groups, while the group with the highest $|\lambda|$ values has many more smaller FRs. We interpret this result as a selection effect on the duration of observed FRs: for the same duration and velocity, the FRs more inclined along the Sun–spacecraft direction (*i.e.* with higher $|\lambda|$ values because the spacecraft crossing is more aligned along the FR axis) have a smaller radius. We conclude that the breakdown of the power law for the smaller radius, as shown in Figure 1 with the tail of the green curve from Feng *et al.* (2008), is due to a selection effect. Therefore we excluded the FRs with $R < 0.008$ AU from the power-law fit. This selection effect is absent from the MC list of Lepping and Wu (2010), as shown in Figure 2b, where we show similar distributions for different groups of MCs ordered by their related λ .

Other selection effects can play a role in the distribution of the flux ropes. Indeed, the probability of FR detection is proportional to the apparent surface of the FR, which is defined as the surface area of the FR projected onto the sphere centered on the Sun and crossing the spacecraft location (the FR motion is almost along the Sun–spacecraft direction). The

smaller an FR, the smaller its apparent surface, and accordingly the lower its probability of being crossed by the observing spacecraft. The studied FRs are all observed at a distance $D = 1$ AU. The surface of a flux rope projected onto the sphere $r = D$ is $\approx 2RL_p$, where L_p is the length of the axis projection (on $r = D$), and where we assumed a similar radius $[R]$ along the FR axis when observed at 1 AU (as expected from the axial-flux conservation along the flux rope and an approximate total-pressure balance with the surrounding solar wind). This implies that small FRs are under-represented in the FR lists at least by a factor proportional to $1/R$ (Wu, Feng, and Chao, 2008) and probably more, because L_p is expected to be an increasing function of R (see below).

Next, we estimated the probability of detecting an FR. We assumed that the FRs have an equiprobability of presence in the whole range of ecliptic longitude and in a band of latitude $\pm \theta_{\max}$. Indeed, the numerous rotations of the Sun and its associated interplanetary magnetic field, on a time scale of several years, imply that FRs formed either in the corona or in the heliospheric current sheet can be detected at any longitude. However, the equiprobability hypothesis in latitude is more challenging in both formation scenarios, and as such is only the simplest hypothesis. Within this framework, the probability of detecting one FR $[P_{\text{FR}}]$ is the ratio of the solid angles, as seen from the Sun, of the FR and of the latitude band, considered as follows:

$$P_{\text{FR}} = \frac{2RL_p}{4\pi \sin \theta_{\max} D^2}. \tag{4}$$

Then, the distribution dN_{obs}/dR for detected flux ropes needs to be corrected by a factor $1/P_{\text{FR}}$ to estimate the total number of FRs released per year. For small FRs, we currently have no information on L_p , while for MCs the heliospheric imagers indicate that L_p is similar to D (see, e.g., Janvier, Démoulin, and Dasso, 2013 and references therein). We therefore took $L_p = D$ in the following numerical applications. We anticipate that this value is too high for the small FRs because these thin structures are not expected to keep their twisted structure over such large distances, because they can be affected by reconnection with the surrounding solar-wind magnetic field, as found in some MCs (Dasso *et al.*, 2006, 2007; Ruffenach *et al.*, 2012). In particular, L_p is expected to decrease for FRs with smaller R because these flux ropes are more likely to be affected by reconnection because they have a lower axial magnetic flux. For example, if L_p behaves as a power law of R , such as R^{s_L} , the corrected distribution function $[dN_{\text{total}}/dR]$ would have to be multiplied by R^{-s_L} , so that its slope (on a logarithmic scale) would decrease by $-s_L$. Instead, in the following, we implement a conservative correction by correcting dN_{obs}/dR only with R (so we keep $L_p = D = 1$ AU for all FRs). Then, the total distribution $[dN_{\text{total}}/dR]$ of the FRs present at 1 AU per year is a function of R as

$$\frac{dN_{\text{total}}}{dR} = \frac{dN_{\text{obs}}}{dR} \frac{2\pi \sin \theta_{\max}}{R/D}. \tag{5}$$

The range of latitudes $[\pm \theta_{\max}]$ where FRs are present cannot be derived by *in-situ* data but only from coronagraphs and heliospheric imagers. So far, this is only possible for MCs that have been associated with CMEs (Rouillard, 2011, and references therein). The CME latitude range is solar-cycle dependent and to a lesser extent dependent on the CME catalog used (Yashiro *et al.*, 2004; Robbrecht, Berghmans, and Van der Linden, 2009). Moreover, the measured CME latitudes are subject to strong projection effects (when they are not ejected near the limb) and the data are providing only an upper limit on the true latitude of a CME. Locating the source regions of CMEs allows us to better define the latitude distribution of CMEs. The CME source regions are typically found in the active-region belt, which extends to $40^\circ - 50^\circ$ latitude in both hemispheres with a shift to lower latitude during the

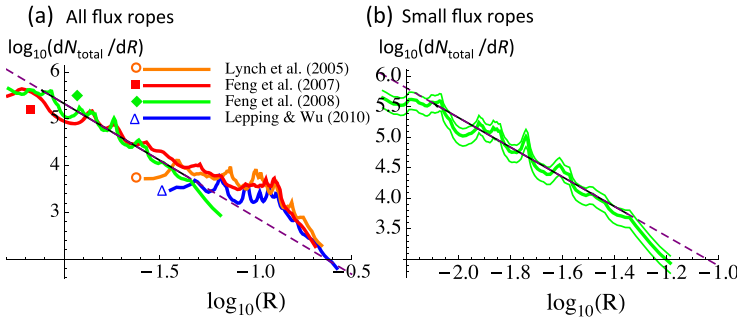


Figure 3 FR distributions, corrected for the FR surface-selection effect, versus the FR radius on log–log scales. (a) The continuous black straight line is the fit of the distribution of small FRs from Feng *et al.* (2008) within the radius range [0.008, 0.05] AU. The fit is extended beyond the fitting region by the dashed purple line. (b) Corrected distributions for small FRs (Feng *et al.*, 2008). The central curve, also shown in (a), is surrounded by the distributions computed with $N_{\text{part}} \pm \sqrt{N_{\text{part}}}$, where $N_{\text{part}} = 10$ is the number of FRs in each partition, to show the effect of statistical fluctuations in each partition.

solar cycle (see Cremades and Bothmer, 2004, Figure 9; Tripathi, Bothmer, and Cremades, 2004, Figures 11, 16, and 18; Howard, Nandy, and Koepke, 2008, Figure 2c; Wang *et al.*, 2011, Figures 3 and 4a). However, not all CMEs are moving out radially, and moreover, some are deflected by nearby coronal holes, especially towards the Equator during solar minimum (Cremades and Bothmer, 2004; Cremades, Bothmer, and Tripathi, 2006; Wang *et al.*, 2011). This implies that the distribution of source regions is only an approximation of the distribution of the CME propagation directions. In the following results, we used $\theta_{\text{max}} = 45^\circ$ as an estimate of the mean extension of the CME propagation direction. Taking into account these limitations, the quoted numbers would simply need to be multiplied by a factor 0.8 (resp. 1.4) if $\theta_{\text{max}} = 30^\circ$ (resp. 60°) were used instead.

5. Corrected Population of Small Flux Ropes

The distributions corrected for the biases described in Section 4 are shown in Figure 3, and they show that small FRs are much more numerous than large ones, especially MCs. The power law is steep with a slope of -2.4 ± 0.14 where the slope error is computed with a confidence level of 95 %. This means that for a decrease of R by a factor of ten there are ≈ 250 times more FRs. Moreover, in the present data, there is no indication that the power law would stop at the lowest radius shown (0.005 AU) since the flattening of the distribution for low R -values was identified as a bias due to a selection of the axis orientation (Figure 2). There is no indication either that the power law stops, or that its slope changes at higher R -values before being covered by the MC distribution.

A closer look at Figure 3a shows a possible temporal evolution of the power-law slope: a shallower slope is computed from the list of Feng, Wu, and Chao (2007) (red curve in Figure 3a) than the one computed from the more extended list of Feng *et al.* (2008) (green curve in Figure 3a). To investigate this temporal effect more thoroughly, we split the list of Feng *et al.* (2008) into three temporal intervals with a similar number of small FRs. Keeping the same range of $\log_{10} R$ for the fit, we found slopes of -1.8 ± 0.1 , -2.1 ± 0.5 , and -3.4 ± 0.3 for the temporal ranges [1995, 1997], [1998, 2001], and [2002, 2005], respectively. This indicates a plausible temporal evolution of the power-law slope. However, a much larger

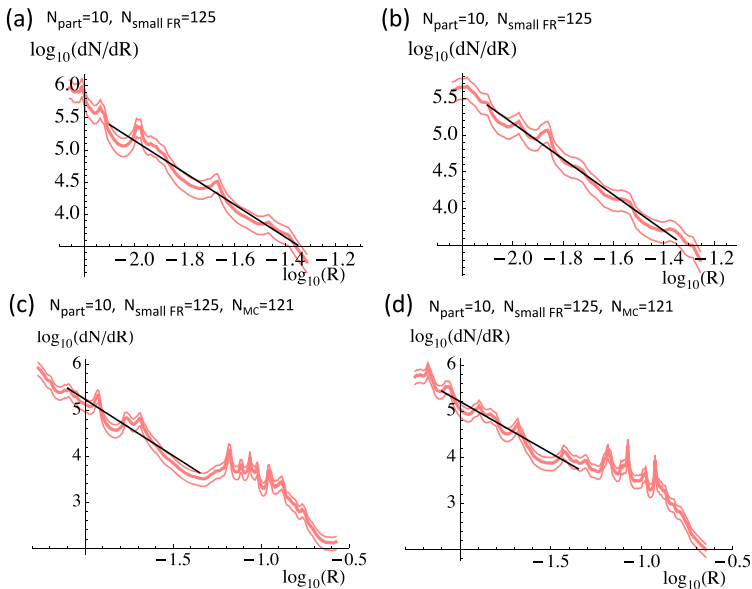


Figure 4 (a, b) Tests with a power-law distribution $R^{-2.4}$ analyzed in the same way as the observations (Figure 3). Panels a and b are two different realizations with the same number of cases and partitions as in the observations. The central curves are surrounded by the distributions computed by $N_{\text{part}} \pm \sqrt{N_{\text{part}}}$ to show the effect of statistical fluctuations in each partition. (c, d) Other realizations with a Gaussian distribution in $\log_{10}(R)$ added to simulate MCs (mean value at $\log_{10}(R) = -1$ and standard deviation = 0.16). They show a similar amplitude of fluctuations as the observed distributions shown in Figure 3.

number of small FRs studied over a much longer period of time would be needed to confirm this and to test whether this evolution is related to the solar cycle.

To complete the study of the observed distributions of flux ropes in the solar wind, we tested the partition technique used so far to derive dN_{total}/dR with a power-law distribution $[R^{-s}]$ generated by a random generator. We set the range of R to the observed range of flux-rope radius from the list of Feng *et al.* (2008) (Figure 3b) and $s = -2.4$ so that the tests are directly comparable with the observations. For a larger number of cases in the synthetic distribution, the slope of the fit becomes closer to $s = -2.4$ and the estimated error on the fitted slope decreases accordingly, as expected.

The most relevant test consists of a number of cases similar to the number of observed FRs. Therefore we selected $N = 125$ to compare with the results obtained with the list of Feng *et al.* (2008). The tests are also shown with the same number of cases per partition $[N_{\text{part}}]$ as for the observations. The results of two typical tests of the theoretical distributions are shown in Figures 4a, b. From the fitting of the curves, the slope value is generally found to be around -2.4 with a variation from case to case by less than 0.2. The test results also show statistical fluctuations of dN/dR . They are similar in magnitude to those presented in Figure 3b, showing that fluctuations such as the bump in the middle of the distributions have no physical meaning. They can be reduced by increasing the N_{part} value without any significant effect on the derived slope (within the error bar quoted above). We also performed other tests changing s , N_{part} , the range of R studied, and the number of cases. All of these results show that the partition technique is a robust technique to derive the dN/dR distribution, especially when it is a steep function over a broad range of R -values.

As a final step, we also compared the partition technique used above with the more classical histogram technique: binning both the observed and synthetic data with N_{bin} bins of same extension in R . We found slopes similar to those quoted above, but with much larger uncertainties, typically larger by a factor three to eight. These larger uncertainties with a classical histogram are due to the bins with high R values, which have a small count number, which means large statistical fluctuations. With a histogram, the slope is also sensitive to the location of the bin boundaries as well as their number [N_{bin}]. For example, the slope changes from -2.8 to -2.5 when N_{bin} is changed from 5 to 20 for the data of Feng *et al.* (2008), while the slope reaches -1.95 for $N_{\text{bin}} = 40$. In contrast, the slope is not significantly affected by N_{part} with the partition technique (it changes by less than 0.1 when N_{part} is changed from 5 to 40). This conclusion was also extended to the theoretical distributions described above. We conclude that the partition technique is the best to analyze dN/dR , a logical conclusion since it optimizes the distribution of the small number of observed FRs in the partitions.

6. MC-Only Distributions

In the original distribution of flux ropes (Figure 1), the large flux ropes, *i.e.* the MCs, stand above the power-law distribution of the small FRs and within a large bump. This bump remains even after correcting the observed distribution (see Figure 3a). This bump is both higher and broader in R than the fluctuations due to the small statistics in the partitions (with similar fluctuations in observations, Figure 3, and in theoretical tests, Figure 4).

The dN_{total}/dR distributions of MCs obtained from different lists are evaluated per year and therefore can be compared. The three data sets have a similar global distribution, especially from the lists of Lynch *et al.* (2005) and Feng, Wu, and Chao (2007), which have the closest time range ([1995, 2003] and [1995, 2001], respectively). The distribution of Lepping and Wu (2010) is close to the previous ones only for $R \gtrsim 0.12$ AU (Figure 3a). For lower values of R , the distribution becomes lower by about a factor two. This can be partly explained with a temporal evolution as follows: we first limited Lepping's list to 2001 (2003) to make it directly comparable with the time period of Feng, Wu, and Chao (2007) and Lynch *et al.* (2005). Then, with the same time interval, dN_{total}/dR for the three MC lists is more similar (within the statistical fluctuations) for $R \gtrsim 0.08$ AU. On the other hand, for $R \lesssim 0.08$ AU, the dN_{total}/dR distribution of Lepping's list is very similar to the power-law distribution of the small FRs, while the two other distributions are still much higher (similar to Figure 3a). This indicates a selection effect compared with the lists of Lynch *et al.* (2005) and Feng, Wu, and Chao (2007). These last authors have probably also included as MCs some of the cases considered as MC-like by Lepping, Wu, and Berdichevsky (2005). In other words, Lepping and Wu (2010) have set more restrictive conditions on the definition of MCs. Such disagreements among independent lists of MCs could have several origins, as summarised in the introduction of Lepping, Wu, and Berdichevsky (2005).

Next, we extended the modeled distribution function of Section 5 by adding to the synthetic power law 121 cases to represent the MCs with a Gaussian distribution in $\log R$ (Figures 4c, d). Various realizations of this distribution show fluctuations of the same order as in Figure 3a; according to this, peaks in the MC region are also caused by statistical fluctuations.

The comparison of lists, detailed above, shows an ambiguity in identifying an event as a small FR or as an MC within an intermediate range of radius (about $R = 0.05$ AU). A possible way to remove this ambiguity is to perform a precise case-by-case analysis, specifying

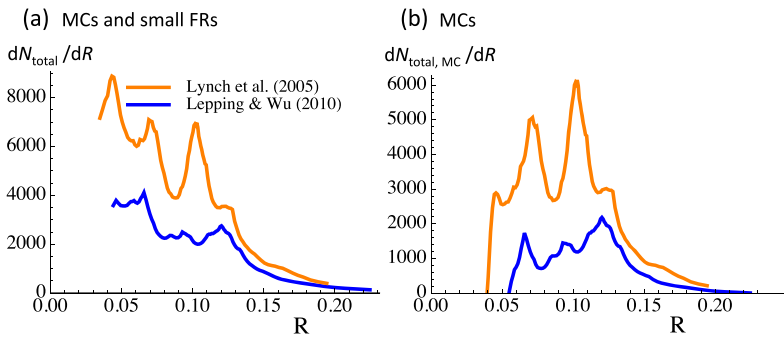


Figure 5 FR distributions corrected for the FR-surface-selection effect *versus* the FR radius. We chose $N_{part} = 20$ to limit statistical fluctuations. (a) Distributions with all the FRs present in the reported lists. (b) A power-law fit to the small FRs (shown in Figure 3b) is subtracted from the distribution shown in panel a. Panel b shows an estimate of the distribution limited to MCs alone (the different peaks probably come from statistical fluctuations, see Section 6).

that an MC is required to have a proton temperature significantly lower than the mean proton temperature found in the solar wind traveling at the same speed. By significant, we mean that a factor of two can be used, as typically used more generally for ICMEs (Richardson and Cane, 2010). A second arbitrary parameter that has to be chosen is the fraction of the total number of FRs such that this condition on temperature should hold to define an MC. The splitting between small FRs and MCs will depend on the values adopted for these parameters. Here we instead took a statistical approach to separate the two distributions, which we describe below.

Since there is no indication in the data that the power law found for small FRs (Figure 3) is ending (or changing slope) before the radius range of MCs, we assumed that this power law extends to higher R values than the fit range used to derive it. We subtracted this power law from the global dN_{total}/dR distribution to estimate only the distribution of MCs [$dN_{total,MC}/dR$]. Both the Lynch and Lepping lists have Gaussian-like distribution for $dN_{total,MC}/dR$ (Figure 5b) when plotted with linear scales. This contrasts with the total FR distributions, which have a large tail on the small R side (Figure 5a). The mean values (0.094 and 0.11 AU) and standard deviations (0.026 and 0.02 AU) of $dN_{total,MC}/dR$ are similar. The main difference is the magnitude of $dN_{total,MC}/dR$, as earlier described in log–log plots (Figure 3a).

Again, this statistical study, which aims at providing the distribution of observed MCs, gives strong evidence that small flux ropes and larger ones, *i.e.* MCs, are of different origin.

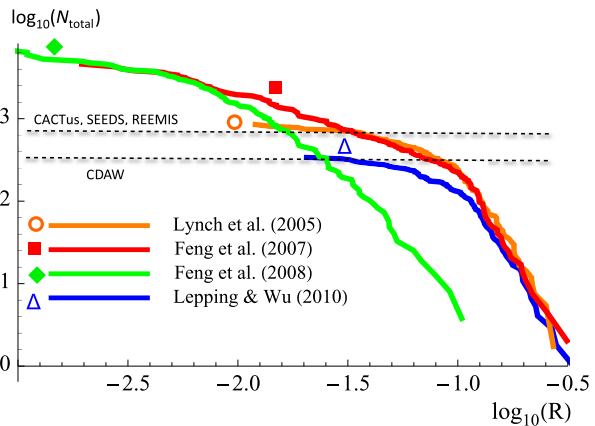
7. Are MCs and/or Small FRs Related to CMEs?

We first investigated the cumulative function of cases per year [$N_{total}(R)$], summing the cases from the larger to the lower radius, as

$$N_{total}(R) = \int_R^{R_{max}} \frac{dN_{total}}{dR} dR. \tag{6}$$

The summation of cases was performed starting from the larger ones [$N_{total}(R_{max}) = 0$] to lower radius values because there are fewer FRs with larger radius, *i.e.* with this definition the larger FRs are not covered by the smaller FRs in the summation of cases. We only present

Figure 6 Cumulative distribution functions of the number of events [N_{total}] computed per year with an average over the time period of the lists. The number of events in all curves is corrected for the FR apparent surface, Equation (5), and the summations are made from the larger to the smaller radius, Equation (6). The number of FRs per year estimated from the CME catalogs are shown as dashed black lines (see Table 1 for values).



the results already corrected for the apparent FR surface bias (*i.e.* with dN_{total}/dR). As expected from the dN_{total}/dR curves (Figure 3a), the $N_{\text{total}}(R)$ curves, derived from lists with MCs, have similar values for the broader range of R corresponding to large MCs (Figure 6). The results of Lynch *et al.* (2005) and Feng, Wu, and Chao (2007) almost agree down to $R \approx 0.025$ AU, while the results from Lepping and Wu (2010) are significantly lower for small R (factor ≈ 2). Finally, as expected, the total number of FRs is dominated by the smaller ones (Feng's lists).

Next, we compared the above total number of FRs per year with the corresponding total number of CMEs observed during the same period of time. This required estimating the number of FRs expected from the observed number of CMEs. Recent studies concluded that a large portion (Vourlidas *et al.*, 2013) or even most of the CMEs (Gopalswamy *et al.*, 2013; Mäkelä *et al.*, 2013) have a flux-rope structure. The CMEs observed *in-situ* (ICMEs) without flux ropes would be cases crossed by the spacecraft close to the FR boundary, or even outside the FR (*e.g.* Jian *et al.*, 2006). The fraction of MCs found in ICMEs is solar-cycle dependent, and we used the yearly fraction found by Richardson and Cane (2010) to convert the observed number of CMEs into the predicted number of FRs.

The early number of CMEs is counted by at least four catalogs. The first catalog is the Coordinated Data Analysis Workshop (CDAW), which relies on visual analyses of SOHO/LASCO images by operators (Yashiro *et al.*, 2004). The next three catalogs are based on different computer algorithms to track the brightness evolution in coronagraph images. They are the Computer Aided CME Tracking (CACTus: Robbrecht, Berghmans, and Van der Linden, 2009), the Solar Eruptive Event Detection System (SEEDS: Olmedo *et al.*, 2008), and the Automatic Recognition of Transient Events and Marseille Inventory from Synoptic maps (ARTEMIS: Boursier *et al.*, 2009). Each catalog has its own bias, as described in the references and by Yashiro, Michalek, and Gopalswamy (2008). Typically, the algorithm-based catalogs detect more and fainter CMEs, and some are considered as incorrect detections by CME experts.

From these catalogs we computed an estimate of the number of FRs as follows: Since the LASCO coronagraph was not working in 1995, there are no CME data. However, the CME rate correlates closely with the sunspot number (Robbrecht, Berghmans, and Van der Linden, 2009), which was at a similar mean level in 1995 and 1997, therefore we duplicated the data of 1997 for 1995 (in any case, the expected number of CMEs in 1995 is smaller than in the years after 1998, so this represents a small correction). For the years 2008 and 2009, Richardson and Cane (2010) found no MCs, so there is no need for CME counts for

Table 1 Predicted total number (rounded values) of FRs ejected from the Sun per year during four time periods (corresponding to the FR lists, see the sixth column). The estimates are based on four CME catalogs: CDAW, CACTus, SEEDS, and ARTEMIS (see Section 7). The last column presents the highest values of the cumulative function of N_{total} shown in Figure 6, averaged per year during the time period indicated, *i.e.* the estimated total number of FRs per year at 1 AU.

| Time period | CDAW | CACTus | SEEDS | ARTEMIS | Reference of FR list | N_{total} |
|-------------|------|--------|-------|---------|----------------------------|--------------------|
| 1995–2003 | 330 | 790 | 740 | 720 | Lynch <i>et al.</i> (2005) | 850 |
| 1995–2001 | 290 | 680 | 610 | 630 | Feng, Wu, and Chao (2007) | 4600 |
| 1995–2009 | 370 | 680 | 580 | 510 | Lepping and Wu (2010) | 390 |
| 1995–2005 | 330 | 760 | 710 | 660 | Feng <i>et al.</i> (2008) | 7040 |

these two years to predict the FR number. From these data, the predicted number of MCs was computed per year and summed for the time interval of the FR lists (Table 1, columns 2–5). The results with the algorithm-based catalogs are very similar because the catalogs detected a similar number of CMEs (Boursier *et al.*, 2009).

Next, we compared the mean value per year of the predicted number of FRs from the number of CMEs in catalogs (Table 1, columns 2–5) with the *in-situ* observed and corrected number of FRs (Table 1, column 6). A close match is found between the numbers predicted from CDAW and derived from Lepping's list (370 and 390, respectively). A fair match is also found between the numbers predicted from CACTus, SEEDS, and ARTEMIS (790, 740, and 720, respectively) and derived from Lynch's list (850). The predicted yearly averaged numbers of FRs depend more on the type of catalog (manual/algorithm based) than on the period of time analyzed (Table 1). Uncertainties on the number of CMEs/FRs present in both CME catalogs and MCs lists is due to the thresholds implemented, which are more or less conservative depending on the authors' choice. This leads to a factor \approx two between the different estimates of the number of CMEs/MCs. We also recall the use of Equation (5) with $\theta_{\text{max}} = 45^\circ$ to correct the observed number of FRs. The quoted numbers would be simply multiplied by a factor 1.4 (resp. 0.8) if the extreme values $\theta_{\text{max}} = 30^\circ$ (resp. 60°) were used instead, so this has a weaker effect than the factor two quoted above. Indeed, in the logarithm scale of Figure 6a, this corresponds to a shift of the curves of 0.15 upward and 0.1 downward, respectively, which means a small shift compared with the variations of $\log N(R)$.

In contrast to the case of MCs, the number of small FRs is much too large compared with the number of FRs predicted by the CME catalogs, by a factor between 7 and 21 (Table 1). This conclusion is supported by the following two points: first, the fact that algorithm-based detections of CMEs have a fraction of false detections or split some events into several (Yashiro, Michalek, and Gopalswamy, 2008) implies that the quoted prediction of FRs in Table 1 with CACTus, SEEDS, and ARTEMIS are expected to be overestimated. Second, there is no evidence that the power law found for small FRs would end or change to a lower slope at smaller radius (Section 5), then even more small FRs would be expected at smaller scales. A way to decrease the number of small FRs would be to drastically reduce θ_{max} . However, if these small FRs are of solar origin, as argued in Section 8, both blowout jets and streamers have a broad range of latitudes, therefore θ_{max} cannot be small. These two points imply that the predicted number of small FRs in Table 1 (column 7) from Feng *et al.* (2008) is expected to be a lower bound.

In summary, the number of CMEs found with an algorithm-based catalog is expected to be an overestimation, while the number of small FRs is expected to be an underestimation. Because the number of estimated FRs from CMEs is a factor \approx ten times lower than the

number of small FRs, and this factor is expected to be even higher as argued above, we conclude that the small FRs are not related to CMEs, even when including the narrow CMEs. On the contrary, the predicted number of FRs from the CME catalogs match the corrected number of MCs within a factor two of uncertainty (depending on the strictness of the criteria to define both a CME and a MC). We conclude that only the MCs, with a Gaussian-like distribution of radius, are the counterparts of all CMEs.

8. What Are the Origins of the Small Flux Ropes?

Several scenarios for the formation of small flux ropes are possible, as we describe below.

First, lower in the solar atmosphere, blowout X-ray jets are jets with particular characteristics, such as the ejective eruption of the magnetic arcade at their base (Moore *et al.*, 2010). The destabilization of a closed-field configuration inferred in such processes is similar to that of the initiation of CMEs, the main difference being that reconnection takes place with an open magnetic field. This so-called interchange reconnection removes parts of the overlying arcade, decreasing the downward magnetic tension, and then allowing the core to erupt in a jet-like manner. MHD simulations reproducing the main characteristics of these blowout X-ray jets involve shearing motions of an arcade, or the emergence of a twisted flux tube, in an open-field environment (Pariat, Antiochos, and DeVore, 2010; Archontis and Hood, 2013). Evidence of the ejections of a flux rope is found both in these simulations and in observations (Liu *et al.*, 2011; Moore *et al.*, 2013). Then, while CMEs typically originate from the core of closed-field regions so that the erupting core should have enough magnetic flux to make its way through the overlying stabilizing field, a small magnetic bipole can have an ejective eruption if it is located in an open-field environment. Since smaller magnetic bipoles are much more numerous than larger ones, blowout X-ray jets are natural candidates to be the origin of small FRs in interplanetary space.

Second, there is observational evidence of the ejection of plasma blobs from above the cusp of streamers (Sheeley *et al.*, 1997, 2009; Wang *et al.*, 2000; Song *et al.*, 2009). With STEREO imagers, these plasma blobs can be tracked into the inner heliosphere (Sheeley and Rouillard, 2010; Rouillard *et al.*, 2010). These transients have a wide range of sizes, and some show evidence of a twisted magnetic structure. They are therefore good candidates to be the origin of small FRs. Three-dimensional MHD simulations, with settings tuned to the configuration above streamers, localize the main instability very close to the streamer cusp (Chen *et al.*, 2009). Therefore reconnection in the current sheet above streamers, with the presence of a guiding field along the current sheet, is also a candidate to be the origin of small FRs in interplanetary space. Indeed, MHD simulations show the formation of flux ropes from the development of the tearing mode (Einaudi *et al.*, 2001). More complex cases, involving several current sheets modeling adjacent helmet streamers, show the development of multiple tearing modes with growth rates much higher than the simple tearing-mode prediction (Dahlburg and Karpen, 1995). In their simulation, Dahlburg and Karpen (1995) showed that such a mechanism can lead to the formation of plasmoids with size scales between 3.5×10^{-5} AU and 3.5×10^{-3} AU when present at 1 AU. This upper limit agrees with the lower limit of very small flux ropes observed (Figure 1). However, the origin of small flux ropes with larger sizes remains to be investigated.

A plausible alternative for the formation of small FRs farther away from the Sun is the hypothesis that they originate from the heliospheric current sheet (HCS: Moldwin *et al.*, 2000). In this scenario, the small FRs would result from multiple reconnections during the development of the tearing instability in the HCS. This process is similar to that advocated

for the FR formation above streamers and for those observed in Earth's magnetotail (Linton and Moldwin, 2009 and references therein). However, similarly as for simulations for helmet streamers, the thickness of the HCS is too small to clearly explain the formation of structures as large as 0.05 AU: the HCS is $\approx 10^4$ km at 1 AU, so smaller than 10^{-4} AU (e.g. the review of Smith, 2001, and more recently Blanco *et al.*, 2006). This is ten times smaller than the smallest FRs detected.

Recently, efforts have been made in numerical simulations to investigate the properties of plasmoid chains, formed by the nonlinear development of the tearing instability in current sheets. This development results in coalescence of plasmoids to form larger structures. A theoretical approach to the merging of these structures has linked the island half-size [w_{isl}] with the reconnection rate [ϵ] and the system size [L] as follows: $w_{\text{isl}} = \epsilon L$ (Fermo, Drake, and Swisdak, 2010; Uzdensky, Loureiro, and Schekochihin, 2010). This result has been numerically tested by Loureiro *et al.* (2012) for high Lundquist-number plasmas, which is a necessary condition to form plasmoid chains in unstable current sheets (via the plasmoid instability; see Loureiro, Schekochihin, and Cowley, 2007). In this work, the authors showed that the effective reconnection rate is on the order of $\epsilon \approx 0.02$ (independent of the Lundquist number for high values), leading to plasmoids of about $0.02 L$. Then, in the context of HCS, a system size of up to 1 AU can be considered, leading to flux ropes of radius 0.02 AU. Moreover, so-called monster plasmoids can form, whose largest size has been reported to be $\approx 0.1 L$. Interestingly, Loureiro *et al.* (2012) also found a plasmoid population characterized by a distribution function scaling as w_{isl}^{-2} , which is similar to the slope found in the present article for the distribution of small flux ropes (Figure 3). However, it is difficult to conclude with confidence that small flux ropes are of the same nature as plasmoids formed by coalescence of smaller structures in current sheets, both in the HCS and in the coronal streamers. Indeed, simulation-based current sheets present a much simpler configuration than that in the heliosphere. The effect of the solar wind, for example, can stop the growth of FRs by pushing them away from their formation region.

The most straightforward way to test the above three possibilities would be to follow *in-situ* detected small FRs with heliospheric imagers backward in time, and therefore toward the Sun. The main difficulty is that they are typically not seen in imagers because they are both small and not dense enough. Even close to the Sun, the streamer blobs are only 10 % overdense compared with the surroundings. As they expand, while propagating away from the Sun, they have even less contrast, so that following these structures at ≈ 1 AU becomes difficult. A possible way to overcome these difficulties would be to consider small FRs that have been swept by a high-speed stream, which makes them appear as the densest structures (Rouillard *et al.*, 2011). Of the six small FRs studied, only the four largest ones could be followed back to the Sun with the STEREO imagers. Two have been identified as CMEs and the two others as streamers blobs. Their half-size at 1 AU is between 0.025 and 0.06 AU, which means that they are in the intermediate range where both small FR and MC distributions overlap (Figure 1), which is consistent with their mixed solar origin. The last two small FRs studied have a half-size of ≈ 0.01 and 0.02 AU, but we were unable to identify the source of these smaller FRs with imagers.

Another possibility for the source of small FRs is provided by the analysis of the statistical distributions in size of these sources, and these can be compared with the results of Figure 3. However, to our knowledge, none of these distributions are known. At best, one can use the distribution of CMEs that was derived by Robbrecht, Berghmans, and Van der Linden (2009) and that was extended to small-scale eruptions by Schrijver (2010). A power law with a slope ≈ -1.8 was derived for the apparent width of the events, which can be compared with Figure 3 (where the slope is ≈ -2.4). However, there is no bump in the CME

part of the distribution, as would be expected from Figure 3 if MCs were closely associated to CMEs. The two studies also provide solar distributions on the maximum extension of the CMEs. This measurement is generally associated with the extension along the axis of a possible FR within the CME and not with the FR radius. Moreover, the maximum apparent width is affected by projection and selection effects, which are different for coronagraph and EUV imagers. Therefore the distribution of the angular width of the CMEs cannot be directly compared with the distribution of the radius of MCs (from Figure 3), and it requires a much deeper analysis, including modeling, to obtain comparable physical quantities.

Power laws are found in several domains including flare energy, but this has no obvious link with the power law found for small FRs. A plausibly related power law is the one found for the photospheric magnetic field (Parnell *et al.*, 2009 and references therein), as follows: the small bipoles on the Sun emerge and disappear at a rapid rate (with a lifetime typically shorter than a day). For bipoles emerging in an open field, it is plausible that the interchange reconnection occurs a few times, or maybe only once, when the bipole has its maximum extension and before at least one of its photospheric polarities merges with the surrounding network field. Then, if small FRs are formed by blowout X-ray jets, one can envision a close link between the distribution of the photospheric magnetic field and that of small FRs. For CMEs that are mainly coming from ARs, the link is less obvious. First, there is an ongoing debate on the type of distributions for the photospheric magnetic field at the scale of ARs (Zhang, Wang, and Liu, 2010 and references therein). Second, ARs, in contrast to small bipoles, last for a longer time, so that their magnetic configuration can be re-energized after a CME. This implies a broad range of CME numbers launched from ARs, ranging from none to more than 60 (Green *et al.*, 2002; Chen *et al.*, 2011). Therefore, the link between the distributions of the photospheric magnetic field and CMEs, and so MCs, is not direct, and the solar interpretation related to Figure 5 needs developments beyond the scope of this article.

All in all, observational arguments and theoretical/numerical backgrounds are more likely to associate the origin of small FRs to blowout X-ray jets. However, nonlinear developments of tearing modes in the cusp of streamers is a small-FR formation scenario also supported by both observational and theoretical arguments. Moreover, the number of small FRs peaks before crossing the sector boundary (\approx six hours or less; see Figure 9 of Cartwright and Moldwin, 2010a), which agrees with a scenario for the formation of small FRs above streamers. Finally, there is currently no clear argument in favor of formation within the HCS.

9. Conclusion

Following the controversy of whether two populations of FRs exist in the solar wind (Section 1), we investigated the FR distributions from four published lists of events. Detected flux ropes were all fitted by the same flux-rope model, Equation (1), which provided an estimate of the FR parameters such as its radius. Owing to the limited number of observed events in each list (between 121 and 144) and the huge variation of the number of cases along the range of the distributions, histograms classically used for statistical study of distributions are too limited for an appropriate analysis here. Therefore we developed a partition method whose main advantage is that it uniformly spreads the statistical fluctuations across the distribution. This method was broadly tested with theoretical random distributions, in particular for distributions similar to the observed ones. We showed that this new method is indeed reliable even for the limited number of observed FRs currently available (Figure 4).

Investigating possible selection effects on the distributions of the flux-rope radius, we found biases in the observed distributions due to the orientation (Figure 2) as well as to the apparent surface of the detected FRs. We proposed a method applicable to any distribution of flux ropes to correct these biases. After these corrections, we derived the distribution of dN_{total}/dR versus R , where N_{total} is the number of FRs per year at 1 AU and R is the FR radius. We found the following results:

- Two FR populations with different distributions [dN_{total}/dR]: a power law for small FRs and a Gaussian-like for MCs (Figure 3).
- The power law for small FRs [$dN_{\text{total}}/dR \propto R^s$] is a steep function of the FR radius [R] since the slope $s = -2.4 \pm 0.14$ for the period from 1995 to 2005.
- There is evidence that the slope [s] is time dependent, but the number of FRs and the temporal range are both too small to assert a link with the solar cycle.
- The MC distribution is Gaussian-like, closely centered around an FR radius of 0.1 AU with a standard deviation slightly lower than 0.03 AU (Figure 5).
- The distributions of small FRs and MCs overlap around $R = 0.05$ AU. This overlap is limited in radius both because the distribution of small FRs is a steeply decreasing function of R and because it is also the case for the MC distribution for decreasing R values (Figure 3).

Since they have remarkably different distributions, small FRs and MCs probably have different origins. On the one hand, we found that the number of FRs per year predicted from the observed CMEs is close to the observed number of MCs when the observed fraction of MCs in ICMEs is taken into account. More precisely, the predicted number of MCs from the CDAW CME catalog is quite similar to the number of MCs per year in the list of Lepping and Wu (2010), while twice more MCs are predicted from the algorithm-based CME catalogs (CACTus, SEEDS, and ARTEMIS), in agreement with the number of MCs per year in the lists of Lynch *et al.* (2005) and Feng, Wu, and Chao (2007). On the other hand, the small detected FRs are too numerous when compared with the observed CME rates, in particular presenting ratios by at least a factor of ten. These two comparisons of predicted MCs and small flux ropes lead to the conclusion that only the MCs, with a Gaussian-like distribution versus FR radius, are associated with observed CMEs.

Since we showed that the small FRs are not associated with CMEs, even narrow ones, we proposed possible scenarios for the formation of these small FRs. These twisted structures may still originate in other eruptive coronal phenomena such as blowout X-ray jets or multi-reconnection processes, which probably involve nonlinear tearing-mode-like phenomena, in the current sheet at the top of streamers. Both of these scenarios, explaining the solar origin of flux ropes, have some observational and theoretical results that favor either one of these processes to be at the origin of the small FRs observed at 1 AU. At present, a clear answer cannot be given since available instruments are unable to image these small FRs so that one could be able to trace back their propagation from the Sun. A possible approach, beyond the scope of this article, would require the derivation of the distribution of plasmablob radius in the corona and comparing this distribution with that of the size of small FRs derived in this article. Another possible scenario for the formation of small FRs is that they might be formed away from the Sun, in the heliospheric current sheet. Similarly to helmet streamers, this scenario would involve a nonlinear development of the tearing instability in multiple current sheets forming the HCS. Comparisons with simulations of the coalescence of plasmoid chains suggest a similar power law for the distribution of plasmoids as for the FR radius (Figure 3b), as well as sizes of monster plasmoids that might explain the small FR investigated here. However, numerical simulations leave out more complex processes that

involve, for example, the solar wind, so that the formation of small FRs in the HCS remains unclear. To support either of these scenarios, observations will need the capability to track and/or detect flux ropes closer to the Sun. The future *Solar Orbiter* spacecraft should be particularly well suited for these purposes.

Acknowledgements The present work was partially funded by a contract from the AXA Research Fund (MJ) and also supported by the Argentinean grant UBACyT 20020120100220 (SD) and by a one-month invitation of SD by the Paris Observatory. SD is member of the Carrera del Investigador Científico, CONICET. SD acknowledges support from the Abdus Salam International Centre for Theoretical Physics (ICTP), as provided in the framework of his regular associateship.

References

- Archontis, V., Hood, A.W.: 2013, A numerical model of standard to blowout jets. *Astrophys. J. Lett.* **769**, L21. [DOI](#).
- Blanco, J.J., Rodríguez-Pacheco, J., Hidalgo, M.A., Sequeiros, J.: 2006, Analysis of the heliospheric current sheet fine structure: single or multiple current sheets. *J. Atmos. Solar-Terr. Phys.* **68**, 2173–2181. [DOI](#).
- Boursier, Y., Lamy, P., Llebaria, A., Goudail, F., Robelus, S.: 2009, The ARTEMIS catalog of LASCO coronal mass ejections. Automatic recognition of transient events and Marseille inventory from synoptic maps. *Solar Phys.* **257**, 125–147. [DOI](#).
- Cartwright, M.L., Moldwin, M.B.: 2008, Comparison of small-scale flux rope magnetic properties to large-scale magnetic clouds: evidence for reconnection across the HCS? *J. Geophys. Res.* **113**(A12), 9105. [DOI](#).
- Cartwright, M.L., Moldwin, M.B.: 2010a, Heliospheric evolution of solar wind small-scale magnetic flux ropes. *J. Geophys. Res.* **115**, A08102. [DOI](#).
- Cartwright, M.L., Moldwin, M.B.: 2010b, Reply to comment by H.Q. Feng, D.J. Wu, and J.K. Chao on “Comparison of small-scale flux rope magnetic properties to large-scale magnetic clouds: evidence for reconnection across the HCS”. *J. Geophys. Res.* **115**(A14), A10110. [DOI](#).
- Chen, Y., Li, X., Song, H.Q., Shi, Q.Q., Feng, S.W., Xia, L.D.: 2009, Intrinsic instability of coronal streamers. *Astrophys. J.* **691**, 1936–1942. [DOI](#).
- Chen, C., Wang, Y., Shen, C., Ye, P., Zhang, J., Wang, S.: 2011, Statistical study of coronal mass ejection source locations: 2. Role of active regions in CME production. *J. Geophys. Res.* **116**, 12108. [DOI](#).
- Cremades, H., Bothmer, V.: 2004, On the three-dimensional configuration of coronal mass ejections. *Astron. Astrophys.* **422**, 307–322. [DOI](#).
- Cremades, H., Bothmer, V., Tripathi, D.: 2006, Properties of structured coronal mass ejections in solar cycle 23. *Adv. Space Res.* **38**, 461–465. [DOI](#).
- Dahlburg, R.B., Karpen, J.T.: 1995, A triple current sheet model for adjoining coronal helmet streamers. *J. Geophys. Res.* **100**, 23489–23498. [DOI](#). [ADS](#).
- Dasso, S., Mandrini, C.H., Démoulin, P., Luoni, M.L., Gulisano, A.M.: 2005, Large scale MHD properties of interplanetary magnetic clouds. *Adv. Space Res.* **35**, 711–724. [DOI](#).
- Dasso, S., Mandrini, C.H., Démoulin, P., Luoni, M.L.: 2006, A new model-independent method to compute magnetic helicity in magnetic clouds. *Astron. Astrophys.* **455**, 349–359. [DOI](#).
- Dasso, S., Nakwacki, M.S., Démoulin, P., Mandrini, C.H.: 2007, Progressive transformation of a flux rope to an ICME. *Solar Phys.* **244**, 115–137. [DOI](#).
- Démoulin, P.: 2009, Why do temperature and velocity have different relationships in the solar wind and in interplanetary coronal mass ejections? *Solar Phys.* **257**, 169–184. [DOI](#).
- Einaudi, G., Chibbaro, S., Dahlburg, R.B., Velli, M.: 2001, Plasmoid formation and acceleration in the solar streamer belt. *Astrophys. J.* **547**, 1167–1177. [DOI](#).
- Elliott, H.A., McComas, D.J., Schwadron, N.A., Gosling, J.T., Skoug, R.M., Gloeckler, G., Zurbuchen, T.H.: 2005, An improved expected temperature formula for identifying interplanetary coronal mass ejections. *J. Geophys. Res.* **110**, A04103. [DOI](#).
- Feng, H.Q., Wu, D.J., Chao, J.K.: 2007, Size and energy distributions of interplanetary magnetic flux ropes. *J. Geophys. Res.* **112**, A02102. [DOI](#).
- Feng, H.Q., Wu, D.J., Chao, J.K.: 2010, Comment on “Comparison of small-scale flux rope magnetic properties to large-scale magnetic clouds: evidence for reconnection across the HCS?” by M.L. Cartwright and M.B. Moldwin. *J. Geophys. Res.* **115**(A14), A10109. [DOI](#).
- Feng, H.Q., Wu, D.J., Lin, C.C., Chao, J.K., Lee, L.C., Lyu, L.H.: 2008, Interplanetary small- and intermediate-sized magnetic flux ropes during 1995–2005. *J. Geophys. Res.* **113**(A12), 12105. [DOI](#).

- Fermo, R.L., Drake, J.F., Swisdak, M.: 2010, A statistical model of magnetic islands in a current layer. *Phys. Plasmas* **17**(1), 010702. DOI. ADS.
- Gopalswamy, N., Mäkelä, P., Akiyama, S., Xie, H., Yashiro, S., Reinard, A.A.: 2013, The solar connection of enhanced heavy ion charge states in the interplanetary medium: implications for the flux-rope structure of CMEs. *Solar Phys.* **284**, 17–46. DOI.
- Green, L.M., López Fuentes, M.C., Mandrini, C.H., Démoulin, P., Van Driel-Gesztelyi, L., Culhane, J.L.: 2002, The magnetic helicity budget of a cme-prolific active region. *Solar Phys.* **208**, 43–68. DOI. ADS.
- Gulisano, A.M., Démoulin, P., Dasso, S., Ruiz, M.E., Marsch, E.: 2010, Global and local expansion of magnetic clouds in the inner heliosphere. *Astron. Astrophys.* **509**, A39. DOI.
- Howard, T.A., Nandy, D., Koepke, A.C.: 2008, Kinematic properties of solar coronal mass ejections: correction for projection effects in spacecraft coronagraph measurements. *J. Geophys. Res.* **113**, 1104. DOI.
- Janvier, M., Démoulin, P., Dasso, S.: 2013, Global axis shape of magnetic clouds deduced from the distribution of their local axis orientation. *Astron. Astrophys.* **556**, A50. DOI.
- Jian, L., Russell, C.T., Luhmann, J.G., Skoug, R.M.: 2006, Properties of interplanetary coronal mass ejections at one AU during 1995–2004. *Solar Phys.* **239**, 393–436. DOI.
- Kilpua, E.K.J., Jian, L.K., Li, Y., Luhmann, J.G., Russell, C.T.: 2012, Observations of ICMEs and ICME-like solar wind structures from 2007–2010 using near-earth and STEREO observations. *Solar Phys.* **281**, 391–409. DOI. ADS.
- Lepping, R.P., Burlaga, L.F., Jones, J.A.: 1990, Magnetic field structure of interplanetary magnetic clouds at 1 AU. *J. Geophys. Res.* **95**, 11957–11965. DOI.
- Lepping, R.P., Wu, C.C.: 2010, Selection effects in identifying magnetic clouds and the importance of the closest approach parameter. *Ann. Geophys.* **28**, 1539–1552. DOI.
- Lepping, R.P., Wu, C.-C., Berdichevsky, D.B.: 2005, Automatic identification of magnetic clouds and cloud-like regions at 1 AU: occurrence rate and other properties. *Ann. Geophys.* **23**, 2687–2704. DOI.
- Linton, M.G., Moldwin, M.B.: 2009, A comparison of the formation and evolution of magnetic flux ropes in solar coronal mass ejections and magnetotail plasmoids. *J. Geophys. Res.* **114**(A13), A00B09. DOI.
- Liu, C., Deng, N., Liu, R., Ugarte-Urra, I., Wang, S., Wang, H.: 2011, A standard-to-blowout jet. *Astrophys. J. Lett.* **735**, L18. DOI.
- Loureiro, N.F., Schekochihin, A.A., Cowley, S.C.: 2007, Instability of current sheets and formation of plasmoid chains. *Phys. Plasmas* **14**(10), 100703. DOI. ADS.
- Loureiro, N.F., Samtaney, R., Schekochihin, A.A., Uzdensky, D.A.: 2012, Magnetic reconnection and stochastic plasmoid chains in high-Lundquist-number plasmas. *Phys. Plasmas* **19**(4), 042303. DOI. ADS.
- Lundquist, S.: 1950, Magneto-hydrostatic fields. *Ark. Fys.* **2**, 361–365.
- Lynch, B.J., Gruesbeck, J.R., Zurbuchen, T.H., Antiochos, S.K.: 2005, Solar cycle-dependent helicity transport by magnetic clouds. *J. Geophys. Res.* **110**, A08107. DOI.
- Mäkelä, P., Gopalswamy, N., Xie, H., Mohamed, A.A., Akiyama, S., Yashiro, S.: 2013, Coronal hole influence on the observed structure of interplanetary CMEs. *Solar Phys.* **284**, 59–75. DOI.
- Mandrini, C.H., Pohjolainen, S., Dasso, S., Green, L.M., Démoulin, P., van Driel-Gesztelyi, L., Copperwheat, C., Foley, C.: 2005, Interplanetary flux rope ejected from an X-ray bright point. The smallest magnetic cloud source-region ever observed. *Astron. Astrophys.* **434**, 725–740. DOI.
- Moldwin, M.B., Ford, S., Lepping, R., Slavin, J., Szabo, A.: 2000, Small-scale magnetic flux ropes in the solar wind. *Geophys. Res. Lett.* **27**, 57–60. DOI.
- Moore, R.L., Cirtain, J.W., Sterling, A.C., Falconer, D.A.: 2010, Dichotomy of solar coronal jets: standard jets and blowout jets. *Astrophys. J.* **720**, 757–770. DOI.
- Moore, R.L., Sterling, A.C., Falconer, D.A., Robe, D.: 2013, The cool component and the dichotomy, lateral expansion, and axial rotation of solar X-ray jets. *Astrophys. J.* **769**, 134. DOI.
- Olmedo, O., Zhang, J., Wechsler, H., Poland, A., Borne, K.: 2008, Automatic detection and tracking of coronal mass ejections in coronagraph time series. *Solar Phys.* **248**, 485–499. DOI.
- Pariat, E., Antiochos, S.K., DeVore, C.R.: 2010, Three-dimensional modeling of quasi-homologous solar jets. *Astrophys. J.* **714**, 1762–1778. DOI.
- Parnell, C.E., DeForest, C.E., Hagenaar, H.J., Johnston, B.A., Lamb, D.A., Welsch, B.T.: 2009, A power-law distribution of solar magnetic fields over more than five decades in flux. *Astrophys. J.* **698**, 75–82. DOI.
- Richardson, I.G., Cane, H.V.: 2010, Near-earth interplanetary coronal mass ejections during solar cycle 23 (1996–2009): catalog and summary of properties. *Solar Phys.* **264**, 189–237. DOI.
- Robbrecht, E., Berghmans, D., Van der Linden, R.A.M.: 2009, Automated LASCO CME catalog for solar cycle 23: are CMEs scale invariant? *Astrophys. J.* **691**, 1222–1234. DOI.
- Rouillard, A.P.: 2011, Relating white light and in situ observations of coronal mass ejections: a review. *J. Atmos. Solar-Terr. Phys.* **73**, 1201–1213. DOI.
- Rouillard, A.P., Davies, J.A., Lavraud, B., Forsyth, R.J., Savani, N.P., Bewsher, D., Brown, D.S., Sheeley, N.R., Davis, C.J., Harrison, R.A., Howard, R.A., Vourlidas, A., Lockwood, M., Crothers, S.R., Eyles,

- C.J.: 2010, Intermittent release of transients in the slow solar wind: 1. Remote sensing observations. *J. Geophys. Res.* **115**, 4103. DOI.
- Rouillard, A.P., Sheeley, N.R. Jr., Cooper, T.J., Davies, J.A., Lavraud, B., Kilpua, E.K.J., Skoug, R.M., Steinberg, J.T., Szabo, A., Opitz, A., Sauvaud, J.-A.: 2011, The solar origin of small interplanetary transients. *Astrophys. J.* **734**, 7. DOI.
- Ruffenach, A., Lavraud, B., Owens, M.J., Sauvaud, J.-A., Savani, N.P., Rouillard, A.P., Démoulin, P., Foulon, C., Opitz, A., Fedorov, A., Jacquy, C.J., Génot, V., Louarn, P., Luhmann, J.G., Russell, C.T., Farrugia, C.J., Galvin, A.B.: 2012, Multispacecraft observation of magnetic cloud erosion by magnetic reconnection during propagation. *J. Geophys. Res.* **117**(A16), A09101. DOI.
- Schrijver, C.J.: 2010, Eruptions from solar ephemeral regions as an extension of the size distribution of coronal mass ejections. *Astrophys. J.* **710**, 1485–1490.
- Sheeley, N.R. Jr., Rouillard, A.P.: 2010, Tracking streamer blobs into the heliosphere. *Astrophys. J.* **715**, 300–309. DOI.
- Sheeley, N.R. Jr., Wang, Y.-M., Hawley, S.H., Brueckner, G.E., Dere, K.P., Howard, R.A., Koomen, M.J., Korendyke, C.M., Michels, D.J., Paswaters, S.E., Socker, D.G., St. Cyr, O.C., Wang, D., Lamy, P.L., Llebaria, A., Schwenn, R., Simnett, G.M., Plunkett, S., Biesecker, D.A.: 1997, Measurements of flow speeds in the corona between 2 and 30 R sub sun. *Astrophys. J.* **484**, 472. DOI.
- Sheeley, N.R. Jr., Lee, D.D.-H., Casto, K.P., Wang, Y.-M., Rich, N.B.: 2009, The structure of streamer blobs. *Astrophys. J.* **694**, 1471–1480. DOI.
- Smith, E.J.: 2001, The heliospheric current sheet. *J. Geophys. Res.* **106**, 15819–15832. DOI.
- Song, H.Q., Chen, Y., Liu, K., Feng, S.W., Xia, L.D.: 2009, Quasi-periodic releases of streamer blobs and velocity variability of the slow solar wind near the Sun. *Solar Phys.* **258**, 129–140. DOI.
- Tripathi, D., Bothmer, V., Cremades, H.: 2004, The basic characteristics of EUV post-eruptive arcades and their role as tracers of coronal mass ejection source regions. *Astron. Astrophys.* **422**, 337–349. DOI.
- Uzdensky, D.A., Loureiro, N.F., Schekochihin, A.A.: 2010, Fast magnetic reconnection in the plasmoid-dominated regime. *Phys. Rev. Lett.* **105**(23), 235002. DOI. ADS.
- Vourlidas, A., Lynch, B.J., Howard, R.A., Li, Y.: 2013, How many CMEs have flux ropes? Deciphering the signatures of shocks, flux ropes, and prominences in coronagraph observations of CMEs. *Solar Phys.* **284**, 179–201. DOI.
- Wang, Y., Zhang, J., Shen, C.: 2009, An analytical model probing the internal state of coronal mass ejections based on observations of their expansions and propagations. *J. Geophys. Res.* **114**(A13), 10104. DOI.
- Wang, Y.-M., Sheeley, N.R., Socker, D.G., Howard, R.A., Rich, N.B.: 2000, The dynamical nature of coronal streamers. *J. Geophys. Res.* **105**, 25133–25142. DOI.
- Wang, Y., Chen, C., Gui, B., Shen, C., Ye, P., Wang, S.: 2011, Statistical study of coronal mass ejection source locations: understanding CMEs viewed in coronagraphs. *J. Geophys. Res.* **116**, 4104. DOI.
- Wu, D.J., Feng, H.Q., Chao, J.K.: 2008, Energy spectrum of interplanetary magnetic flux ropes and its connection with solar activity. *Astron. Astrophys.* **480**, L9–L12. DOI.
- Yashiro, S., Michalek, G., Gopalswamy, N.: 2008, A comparison of coronal mass ejections identified by manual and automatic methods. *Ann. Geophys.* **26**, 3103–3112. DOI.
- Yashiro, S., Gopalswamy, N., Michalek, G., St. Cyr, O.C., Plunkett, S.P., Rich, N.B., Howard, R.A.: 2004, A catalog of white light coronal mass ejections observed by the SOHO spacecraft. *J. Geophys. Res.* **109**, 7105. DOI.
- Zhang, J., Wang, Y., Liu, Y.: 2010, Statistical properties of solar active regions obtained from an automatic detection system and the computational biases. *Astrophys. J.* **723**, 1006–1018. DOI.